Charge Stabilization in Nonpolar Solvents

M. F. Hsu,† E. R. Dufresne,* and D. A. Weitz

DEAS and Department of Physics, Harvard University, Cambridge, Massachusetts 02138

Received December 31, 2004. In Final Form: March 15, 2005

While the important role of electrostatic interactions in aqueous colloidal suspensions is widely known and reasonably well-understood, their relevance to nonpolar suspensions remains mysterious. We measure the interaction potentials of colloidal particles in a nonpolar solvent with reverse micelles. We find surprisingly strong electrostatic interactions characterized by surface potentials, $|e\zeta|$, from 2.0 to 4.4 k_BT and screening lengths, κ^{-1}, from 0.2 to 1.4 μm. Interactions depend on the concentration of reverse micelles and the degree of confinement. Furthermore, when the particles are weakly confined, the values of $|e\zeta|$ and κ extracted from interaction measurements are consistent with bulk measurements of conductivity and electrophoretic mobility. A simple thermodynamic model, relating the structure of the micelles to the equilibrium ionic strength, is in good agreement with both conductivity and interaction measurements. Since dissociated ions are solubilized by reverse micelles, the entropic incentive to charge a particle surface is qualitatively changed from aqueous systems, and surface entropy plays an important role.

I. Introduction

Charges readily dissociate in polar environments where a large dielectric polarizability lowers the electrostatic barrier to ionization. Consequently, charge is ubiquitous in aqueous systems ($\epsilon \approx 80$) where it impacts important material properties ranging from the electrokinetic response of colloids to the conformation of proteins. When charge resides on the surface of colloidal particles, it helps to stabilize them through repulsive electrostatic interactions, described by the classic theory of Derjaguin, Landau, Verwey, and Overbeek (DLVO).[1,2] The strength and range of the interaction potential play important roles in determining the macroscopic optical and mechanical properties of the material. The range of electrostatic interactions is determined by the ionic strength, which can be robustly controlled through the addition or removal of salt.

In nonpolar solvents ($\epsilon \approx 2$), however, the electrostatic barrier to charging is 40 times larger and much greater than k_BT. Therefore, the common expectation is that charge effects should be inconsequential in thermodynamic equilibrium. However, a number of counterexamples demonstrate that charge can, in fact, play an important role. For example, nonpolar colloids have recently been utilized as electrophoretic ink in flexible electronic displays.[3] Additionally, studies on the stability of soot particles in oil suggest that adding commercial dispersant results in particle stabilization which may include a significant electrostatic component.[4] Furthermore, recent measurements with the surface force apparatus and atomic force microscope have demonstrated repulsive electrostatic forces between surfaces in oil.[5,6]

In all of these examples, surfactants are added to control charging. These surfactants form nanoscale charge-stabilizing aggregates, such as reverse micelles. Experiments over the last 60 years have shown that numerous surfactants impart an electrokinetic response and enhanced stability to nonpolar colloids of many different compositions.[7] Although chemical mechanisms have been identified to explain charge origin in specific systems, a general framework for understanding the origin and effects of charge does not exist. Furthermore, the form of the interactions between charged colloidal particles in nonpolar solvents has not been determined. Knowledge of these effects would enable us to understand charging in nonpolar solvents, predict important properties such as colloid stability and electrokinetic response, and develop strategies for designing new materials.

In this paper, we provide a framework for understanding and controlling charging behavior in nonpolar colloids in the presence of reverse micelles. A thermodynamic model describes ionic strengths and surface potentials as a function of the concentration of reverse micelles from a few material parameters and is consistent with our measurements of interparticle forces, electrophoretic mobilities, and conductivities. We find many surprising parallels to aqueous electrostatics. For example, interactions have the same functional form as those predicted from DLVO theory. Additionally, particle surface potentials are remarkably large, comparable to those of highly charged aqueous colloids. Furthermore, charging is driven by entropy and can be quantitatively described using a thermodynamic energy balance. Notably, we also find striking contrasts to aqueous systems. Screening lengths are about an order of magnitude longer than those readily attainable in water. Therefore, interactions can be stronger than thermal energy over length scales that are many times the particle diameter. In addition, instead of simple ions such as Na^+ or Cl^-, charge carriers are nanoscale reverse micelles. These larger ions have lower ionization energies and enable surfaces to charge by stabilizing their counterions. Furthermore, a finite fraction of reverse micelles spontaneously ionize at room temperature to

* Corresponding author. Present address: Departments of Mechanical Engineering, Chemical Engineering, and Physics, Yale University, New Haven, CT. E-mail: eric.dufresne@yale.edu.

† Present address: General Electric Global Research, Niskayuna, NY.

(1) Derjaguin, B. V.; Landau, L. *Acta Physicochim. URSS* **1941**, *14*, 633.

(2) Verwey, E. J. W.; Overbeek, J. T. G. *Theory of the Stability of Lyophobic Colloids: The Interactions of Sol Particles Having an Electric Double Layer*; Elsevier: 1948.

(3) Comiskey, B.; Albert, J. D.; Yoshizawa, H.; Jacobson, J. *Nature* **1998**, *394*, 253.

(4) Pugh, R. J.; Matsunaga, T.; Fowkes, F. M. *Colloids Surf.* **1983**, *7*, 183.

(5) Briscoe, W. H.; Horn, R. G. *Langmuir* **2002**, *18*, 3945.

(6) McNamee, C. E.; Tsujii, Y.; Matsumoto, M. *Langmuir* **2004**, *20*, 1791.

(7) Morrison, I. D. *Colloids Surf., A* **1993**, *71*, 1.

10.1021/la046751m CCC: $30.25
Published on Web 04/16/2005

contribute to the screening of particle interactions. Finally, the encapsulation of charge within micelles qualitatively changes the thermodynamic balance of energy and entropy that determines surface charge.

II. Materials and Methods

A. Reverse Micelle Solutions. We study solutions containing aerosol-OT (AOT, or sodium di-2-ethylhexylsulfosuccinate), a surfactant with a sulfonate group on its polar head and two branched hydrocarbon tails. Above its critical micellar concentration (cmc) of about 1 mM in dodecane,[8] AOT forms nanometer-sized micelles containing about 30 surfactant molecules.[9] Dynamic light scattering and vapor pressure osmometry experiments have shown that the characteristic size of AOT micelles does not change over a wide range of temperatures and concentrations from about 10 to 100 mM; the hydrodynamic radius, a_h, of dry micelles is about 1.5 nm.[10,11] However, because AOT is very hygroscopic, ambient moisture can greatly affect micelle size; when the AOT/water mass ratio is unity, the molecular weight of micelles becomes more than an order of magnitude larger than that of dry micelles.[9] To obtain reproducible results, it is essential to prepare samples in an environment where moisture is controlled. Therefore, we prepare our samples in a dry glovebox. However, this precaution does not remove water that is in the reagents as received from the manufacturers: batch analysis indicates that about 1 wt % of AOT (Aldrich, 98%) is water and dodecane (Aldrich, 99%) contains at most 0.003% water. Previous light scattering measurements[10] show that a_h varies roughly linearly with the ratio of water to AOT molecules, w_0, up to $w_0 \approx 10.6$. In our experiments, we estimate that $w_0 < 0.6$ for AOT concentrations of up to 200 mM. Assuming all of the water in the dodecane becomes encapsulated within the micelles, we expect a_h to increase slightly to about 1.6 nm.

B. Colloidal Particles. We use poly(methyl methacrylate) (PMMA) particles of radius $a = 780$ nm synthesized by Andrew Schofield (University of Edinburgh). These particles have poly-(12-hydroxy-steric acid) (PHSA) grafted to their surface to provide steric stabilization in nonpolar solvents.[12] Particles are cleaned via multiple cycles of centrifugation, removal of supernatant, and resuspension in clean dodecane. We prepare and store samples in a dry glovebox to prevent micelle swelling and ensure reproducibility. We add particles to AOT/dodecane solutions in a dry glovebox, where they equilibrate for at least 2 days before measurements.

C. Interaction Measurements. We measure electrostatic interactions by analyzing the equilibrium structure of a quasi-two-dimensional ensemble of particles. Particles are confined in wedge-shaped sample cells, consisting of two 75 mm long glass microscope slides in contact at one end and separated by a 13 μm thick Mylar spacer at the other end. Confinement volumes are effectively flat: the change in thickness over the field of view is less than 1% of the average thickness in the regions we analyze. To simplify the interpretation of our results, we prepare the slide surface to be identical to the particle surface. Prior to cell assembly, we spin-coat slides with a 300 nm thick film of PMMA (MicroChem 495PMMA-C4 resist), bake the slides at 120 °C to drive off the solvent, and adsorb PHSA onto the PMMA films by immersing the slides overnight in a 1% solution of PHSA stabilizer in dodecane.[12] We then rinse copiously with dodecane to wash off excess stabilizer, blow-dry the slides with purified nitrogen, and assemble the cells. To prevent uptake of water from ambient humidity, we fill and seal the cells inside the glovebox. We take particular care to prevent contact between particle suspensions and uncured epoxy. Before measurements, we allow the cells to equilibrate for at least 2 days after filling and sealing.

After sample preparation, we capture many statistically independent images of interacting particle ensembles. Images are obtained with bright-field microscopy using a long-working-distance 63×/0.70NA air objective. For each run, we capture a series of images from the same cell region, waiting 1−3 min between images. This is the time needed for particles in our dilute suspensions to diffuse an average interparticle separation.[13] We assume that this time is sufficient to yield independent images for ensemble averaging. We typically locate about 4×10^4 particle positions per run: 200 images with about 200 particles each. Particle number densities range from 0.033 to 0.046 μm^{-2}. To ensure satisfactory confinement to two dimensions, we image particles in thin regions of the sample cells where we observe little out-of-plane motion. In all cases, systematic errors in the apparent particle separation due to out-of-plane motion are less than 3%. Furthermore, to ensure that stuck particles or defects on the surface of the cell do not interfere with our measurements, we calculate the in-plane particle distribution for each experiment and analyze only runs that exhibit a homogeneous in-plane particle distribution. Finally, we repeat measurements on the same cells over the course of 3 weeks and find no time dependence.

We extract the pair potential from the ensemble-averaged pair-correlation function, $g(r)$. For each image, we precisely locate each particle in two dimensions[14] and calculate the two-particle radial correlation function, which we average over our ensemble of statistically independent images. In the dilute limit, Boltzmann statistics can be invoked to calculate the potential directly from $g(r)$: $u(r)/k_BT = -\ln g(r)$. However, we conduct our experiments at higher concentrations to obtain reasonable statistics. In this semidilute regime, peaks in $g(r)$ arise from many-particle collisions. To account for these effects, we use the Ornstein−Zernike integral equation with the hypernetted chain approximation for the appropriate particle density to infer $u(r)$ from $g(r)$.[13] This method assumes that forces between particles are pairwise additive. While substantial many-body interactions can occur at high particle number densities,[15] we expect pairwise additive interactions at the relatively low number densities employed in these experiments. Finally, we corroborate these potentials using a two-dimensional Monte Carlo simulation. Inputting the experimental number density and pair potential, we apply the Metropolis algorithm to calculate the pair-correlation function. We then compare the simulated $g(r)$ to the experimental curves.[16]

D. Conductivity Measurements. A commercial meter (Scientifica model 627) is used to measure the conductivity of surfactant solutions. Solution viscosity is measured with a capillary viscometer (Cannon 50). We verify that the micellar solutions are in thermodynamic equilibrium by measuring the conductivity of the suspensions before and after raising the temperature of the solution to 95 °C for several hours. We find identical results before and after thermal cycling.

E. Electrophoretic Mobility Measurements. We measure electrophoretic mobility (Brookhaven Zeta-PALS with solvent resistant electrodes) by driving particles with an ac electric field (160 V/cm at 2 Hz sinusoidal) and detecting the particle velocity from the phase shift of scattered laser light. Phase analysis light scattering can detect particle motions that are only a fraction of light wavelengths, eliminating the need to use excessively large fields that can perturb the system.[17,18] Nevertheless, we vary the voltage by a factor of 2 for each of our measurements to verify that our material is responding linearly. To minimize the invasion of moisture, cuvettes are filled and sealed inside a dry glovebox, transported in a desiccator, and opened only seconds before measurements.

III. Results and Discussion

A. Interparticle Forces. Reverse micelles dramatically alter the structure of our suspensions. In pure dodecane, our PMMA particles reversibly aggregate, as

(8) Mukherjee, K.; Moulik, S. P.; Mukherjee, D. C. *Langmuir* **1993**, *9*, 1727.
(9) Mathews, M. B.; Hirschhorn, E. *J. Colloid Sci.* **1953**, *8*, 89.
(10) Zulauf, M.; Eicke, H.-F. *J. Phys. Chem.* **1979**, *83*, 480.
(11) Eicke, H. F. *Top. Curr. Chem.* **1980**, *87*, 85.
(12) Antl, L.; Goodwin, J. W.; Hill, R. D.; Ottewil, R. H.; Owens, S. M.; Papworth, S. *Colloids Surf.* **1986**, *17*, 67.
(13) Behrens, S. H.; Grier, D. G. *Phys. Rev. E* **2001**, *64*, 050401(R).
(14) Crocker, J. C.; Grier, D. G. *J. Colloid Interface Sci.* **1996**, *179*, 298.
(15) Brunner, M.; Bechinger, C.; Strepp, W.; Lobaskin, V.; von Grunberg, H. *Europhys. Lett.* **2002**, *58*, 296.
(16) Kepler, G. M.; Fraden, S. *Phys. Rev. Lett.* **1994**, *73*, 356.
(17) Miller, J. F.; Schatzel, K.; Vincent, B. *J. Colloid Interface Sci.* **1991**, *143*, 532.
(18) Tscharnuter, W. W. *Appl. Opt.* **2001**, *40*, 3995.

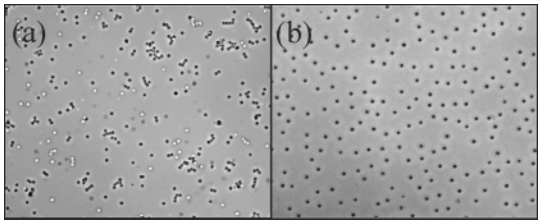

Figure 1. Charge stabilization of a nonpolar suspension: (a) optical micrographs of PMMA particles in pure dodecane and (b) with 12 mM AOT. Field of view: 135 × 108 μm^2.

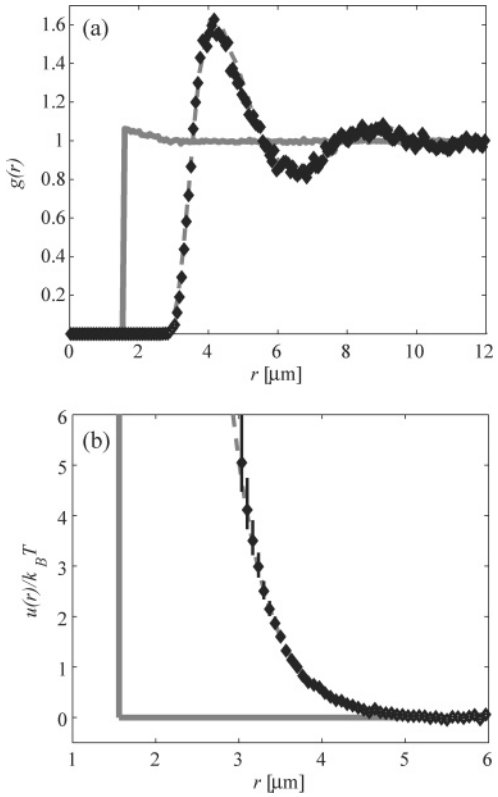

Figure 2. (a) Pair-correlation function, $g(r)$, at 50 mM AOT, $h = 9 \pm 1$ μm, diamonds. Simulated hard-sphere $g(r)$ at the same number density, solid line. Simulated $g(r)$ using the potential extracted from data using the Orstein−Zernike equation, dashed line. (b) Interaction potential, $u(r)$, extracted from the above $g(r)$ using the Orstein−Zernike equation, diamonds. A screened Coulomb fit to the data is plotted as a dashed line. For comparison, a hard-sphere potential is plotted as a solid line.

shown in Figure 1a. However, when AOT is added at concentrations above its critical micellar concentration, the particles disperse. For example, particles in suspensions with 12 mM AOT rarely approach within three particle diameters of each other, as shown in Figure 1b. This micron-ranged repulsion cannot be due to steric forces, since the surfactant molecules and reverse micelles are nanometer-sized.

We quantify this dramatic change in suspension structure using the pair-correlation function, $g(r)$. The pair-correlation function for a 50 mM AOT suspension is shown in Figure 2a. For comparison, we plot $g(r)$ for a suspension of hard spheres at the same number density obtained from a Monte Carlo simulation. The $g(r)$ of simulated hard spheres increases abruptly from zero at contact and exhibits a slight peak, signifying the onset of liquid structure. By contrast, $g(r)$ for our 50 mM AOT suspension remains at zero up to $r \approx 3$ μm, and rises slowly from zero to 1.6 over 1 μm. The form of this pair-correlation function suggests a soft long-ranged potential between particles.

Using the Orstein−Zernike equation, we extract the pair potential, $u(r)$, from the pair-correlation function, as shown in Figure 2b. The interaction is soft and long-ranged: the magnitude of repulsion is greater than k_BT at center−center separations of up to more than two diameters. To verify the potential, we simulate a suspension with this interparticle potential and number density: the resulting $g(r)$ is indistinguishable from our data in Figure 2a. As shown in Figure 2b, the potential $u(r)$ is surprisingly well-fit by a screened Coulomb form:

$$\frac{u(r)}{k_BT} = \left(\frac{e\zeta}{k_BT}\right)^2 \frac{a^2}{\lambda_B} \exp[-\kappa(r - 2a)]/r \qquad (1)$$

where ζ is the zeta potential and κ is the inverse screening length measured from equilibrium interactions. This is the repulsive component of the classic DLVO potential.[1,2] Since our measurements probe interparticle forces when surface-to-surface separations are greater than 500 nm, van der Waals interactions are negligible. Similar measurements in more polar systems ($\epsilon \approx 6$) without surfactant have also found good agreement with DLVO.[19] We extract a dimensionless zeta potential, $|e\zeta_{EQ}|/k_BT = 3.9 \pm 0.4$, and a screening length of about 470 ± 20 nm from the fit. To emphasize that these values are obtained from the equilibrium structure of the material, they are labeled with the subscript EQ. Defying conventional wisdom, this zeta potential is as high as those found in highly charged aqueous systems.[20,21] Using the solution of the linearized Poisson−Boltzmann equation, we can determine an apparent particle charge, Z:

$$Z = \frac{a(1 + \kappa a)}{\lambda_B} \frac{e\zeta}{k_BT} \qquad (2)$$

We calculate a particle charge of about 290 ± 30 electrons. By comparison, highly charged aqueous colloids of comparable size have about 10^4 charges and screening lengths of the order of 10−100 nm.[22]

Interparticle potentials depend sensitively on the cell thickness, h, as shown for the 3.1 mM samples by the symbols and table in Figure 3a.

Nevertheless, each set of points is still well-fit by a screened Coulomb form. As h shrinks from 11.5 to 5 μm, $|e\zeta_{EQ}|$ drops from 4 to 2 k_BT and κ_{EQ} increases from 0.71 to 2.06 μm^{-1}. The variation of κ_{EQ} dominates because of its exponential dependence in the potential. Since our analysis assumes that particles are free to move in only two dimensions, we are unable to investigate interactions in thicker cell regions where particle motion can have a significant out-of-plane component.

Interactions depend strongly on AOT concentration. We measure equilibrium particle structure for a range of AOT concentrations from 3.1 to 200 mM. To best capture the bulk environment, we image each suspension in the thickest regions of the cell that do not show significant out-of-plane motion ($h = 12$, 14, 9, and 5 μm for the 3, 12, 50, and 200 mM AOT suspensions, respectively). We find that the concentration of AOT controls the range of the interaction, as shown in Figure 3b. At 3.1 mM AOT, the interaction is soft and extremely long-ranged, decaying

(19) Royall, C. P.; Leunissen, M. E.; van Blaaderen, A. *J. Phys.: Condens. Matter* **2003**, *15*, S3581.
(20) Behrens, S. H.; Christl, D. I.; Emmerzael, R.; Schurtenberger, P.; Borkovec, M. *Langmuir* **2000**, *16*, 2566.
(21) Crocker, J. C.; Grier, D. G. *Phys. Rev. Lett.* **1994**, *73*, 352.
(22) Crocker, J. C.; Grier, D. G. *Phys. Rev. Lett.* **1996**, *77*, 1897.

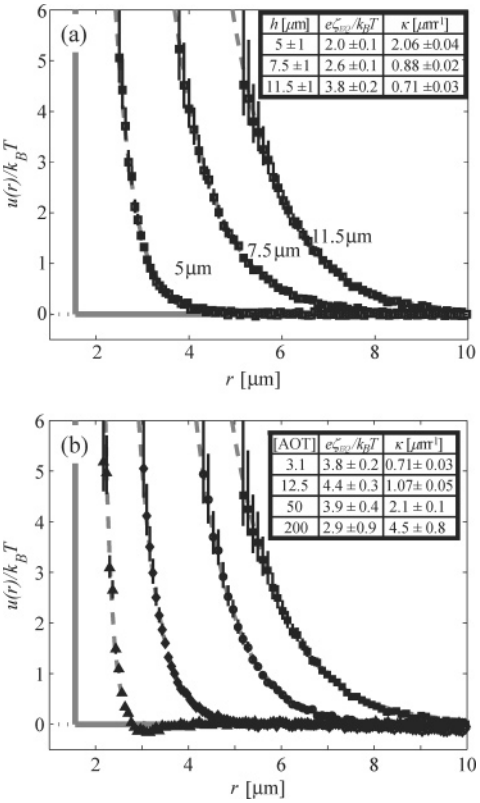

Figure 3. (a) Measured pair potentials, $u(r)/k_BT$, in 3.1 mM AOT solution with varying cell thicknesses, h, as indicated. All potentials are well-fit with a screened Coulomb form, shown as dashed lines; corresponding fit parameters are listed in the inset table. (b) Interaction potentials at different AOT concentrations: squares, circles, diamonds, and triangles represent 3.1, 13, 50, and 200 mM AOT, respectively. Dashed lines indicate screened Coulomb fits to the potentials; corresponding fit parameters are listed in the table.

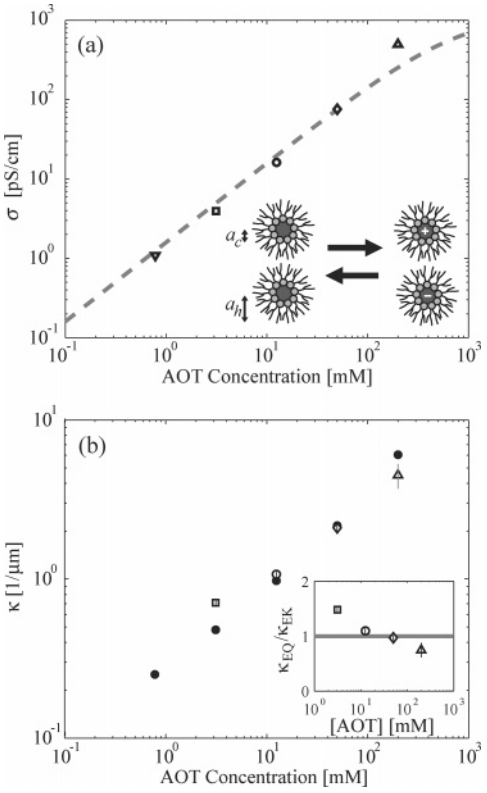

Figure 4. (a) Conductivity of AOT/dodecane solutions without particles. The symbols indicate measurements, and the dashed curve indicates a fit to eq 3 with empirical [AOT]-dependent solution viscosity. Inset: schematic diagram of the two-body process that leads to the creation of charge in the bulk of the solution. (b) Inverse screening lengths as inferred from conductivity, κ_{EK} (solid circles), and interparticle potentials, κ_{EQ} (open symbols). Inset: the ratio κ_{EQ}/κ_{EK} for each concentration of AOT, with a solid line at $\kappa_{EQ}/\kappa_{EK} = 1$ for comparison.

from 6 k_BT at $r = 5$ μm to zero at about $r = 10$ μm. The magnitude of interparticle repulsion is greater than thermal energy up to center-to-center separations of nearly five particle diameters. With increasing AOT concentration, the interaction becomes stiffer and more short-ranged. At the highest concentration of AOT, 200 mM, the potential acquires a shallow minimum at 3 μm. This is likely due to long-range correlations in the structure of the reverse micelle suspension that is also reflected by a sudden growth of viscosity at 200 mM. Apart from this small discrepancy, all of the measured interactions are well-fit by a screened Coulomb form. The implied values of the inverse screening length and surface potential are tabulated in the inset to Figure 3b. As the AOT concentration increases, κ_{EQ} increases from 0.7 to 4.5 μm^{-1}. However, the apparent surface potential varies only weakly with AOT concentration. In fact, our data are consistent with a constant dimensionless zeta potential: $|e\zeta_{EQ}|/k_BT = 4.1$.

Remarkably, these zeta potentials are comparable to those inferred from the interactions of highly charged polystyrene particles in deionized water.[22] Furthermore, the observed screening lengths are much larger than those attainable in water. Together, these observations demonstrate that electrostatic interactions are far from inconsequential. Rather, charge *dominates* suspension structure and stability.

AOT plays an intriguing dual role in our system. When the concentration of AOT is below the cmc, particles aggregate and remain uncharged. Above the cmc, the particles disperse and maintain a large and relatively constant zeta potential. As the concentration of AOT further increases, the screening length shortens. These observations suggest that, above its cmc, AOT affects particle interactions in the same manner as salt, by increasing the ionic strength.

B. Ionic Strength from Conductivity. To elucidate AOT's role in screening electrostatic interactions, we obtain an independent measure of the ionic strength from the conductivity of AOT/dodecane solutions without particles. For same-sized monovalent ions, the conductivity, σ, is given by

$$\sigma = \frac{e^2 n_{ion}}{6\pi\eta a_h} \tag{3}$$

where e is the elementary charge, η is the viscosity, and n_{ion} is the number density of ions. The background conductivity of dodecane is less than 10^{-3} pS/cm, more than 7 orders of magnitude less conductive than standard deionized water. Adding AOT to dodecane at concentrations of 0.8−200 mM yields conductivities from 1.0 to 500 pS/cm, as shown in Figure 4a, a range of more than 2 orders of magnitude. Capillary viscometry measurements show that viscosity increases from 1.40 to 1.77 mPa·s over the same range of AOT concentrations. Combining these results with our estimate of the hydrodynamic radius of the reverse micelles, we apply eq 3 to find that the number density of ionic micelles ranges from 0.16 to 100 μm^{-3}. Furthermore, the fraction of micelles that are ionized is independent of the concentration of AOT: $\chi = n_{ion}/n_{micelle}$

$= 1.2 \times 10^{-5}$. From these measurements of the ion number density, we calculate the inverse screening length, $\kappa = \sqrt{4\pi\lambda_B n_{ion}}$, where $\lambda_B = e^2/4\pi\epsilon\epsilon_0 k_B T$ is the Bjerrum length for monovalent ions. The resulting values of κ_{EK} are plotted against AOT concentration in Figure 4b. To emphasize that these values of the inverse screening length are obtained from electrokinetic measurements, they are labeled with the subscript EK.

Notably, we find good agreement between the screening lengths measured from conductivity and confined interactions, κ_{EQ}, as shown in Figure 4b. However, the discrepancy between κ_{EK} and κ_{EQ} increases at the lowest concentrations of AOT, reflecting the contributions of counterions to screening. We also see discrepancies between these two measures of ionic strength when the particles are strongly confined. We believe that this phenomenon, exhibited in Figure 3a, is driven by electrostatics: since we have prepared the cell walls to mimic the surface of the particles, they should charge to comparable surface potentials. Thus, when wall separations become comparable to the screening length, the counterions from the walls begin to contribute to the ionic environment experienced by the particles.

C. Thermodynamic Model of Bulk Ions. We combine these measurements of ionic strength with simple thermodynamics to reveal the mechanism of ion formation. Both conductivity and interaction measurements show that the number density of ions increases linearly with the concentration of reverse micelles. Therefore, the ratio of ions to micelles, $\chi = n_{ion}/n_{micelle}$, is independent of the concentration of AOT. Furthermore, we find that only a tiny fraction of micelles ionize to form a charge carrier: $\chi = 1.2 \times 10^{-5}$. While weak electrolytes, of the form AB $\rightleftharpoons A^+ + B^-$, can exhibit similar ionization fractions, the law of mass action requires that χ would scale like $[AB]^{-1/2}$. Instead, a charging mechanism where neutral micelles reversibly exchange charge though a collision, $A + A \rightleftharpoons A^+ + A^-$, as shown in the lower right of Figure 4a, leads to a ionization fraction independent of the concentration of A,[7] which is consistent with our data. In equilibrium, the fraction of charged micelles is determined by the difference in free energy between the charged and uncharged states, $\chi = 2\exp(-\Delta F/2k_B T)$. If the free-energy cost of ionizing a single isolated micelle is g_M, then $\chi = 2\exp(-g_M/k_B T)$. Comparing this basic thermodynamic result to our measured value of χ, we find that $g_M = 12\ k_B T$.

The measured micelle ionization energy has a simple electrostatic interpretation. A singly charged conducting sphere of radius a_c surrounded by a dielectric medium has an electrostatic energy, $k_B T\lambda_B/2a_c$.[23] Assuming that electrostatic contributions dominate the ionization free energy and the core of the micelle is effectively a conductor, then our measured value of g_M implies a core radius, $a_c = 1.2$ nm. This is in good agreement with neutron scattering measurements.[24] Thus, we conclude that the equilibrium ionic strength of a solution of reverse micelles is determined by a competition between entropy and electrostatics. The relative size of the Bjerrum length and the micellar core radius determine the charge fraction. When $\lambda_B \gg a_c$, a small fraction of micelles acquire a single fundamental charge. When $\lambda_B \approx a_c$, nearly all of the micelles charge and individual micelles can become multiply charged.

D. Surface Potentials from Electrophoretic Mobility. Interaction measurements suggest that our particles develop remarkably large surface potentials in the presence of reverse micelles. To further elucidate the nature of particle charge, we observe the motion of particles in an electric field. This motion is quantified by the electrophoretic mobility: the ratio of the particle velocity and the electric field. The electrophoretic mobility depends on both the particle surface potential and the distribution of ions in solution. When the hydrodynamic mobility of charge carriers in the bulk of the solution is known, we can combine measurements of conductivity and electrophoretic mobility to calculate the surface potential.

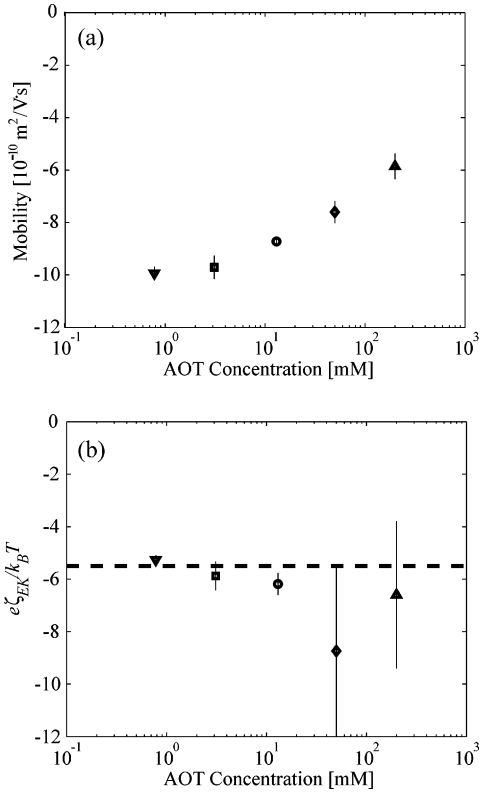

Figure 5. (a) The electrophoretic mobility of PMMA particles in solutions of AOT in dodecane falls in magnitude with increasing AOT concentration. (b) The dimensionless surface potential as a function of AOT concentration. The dashed line indicates −5.5.

Below the critical micellar concentration of AOT, our particles exhibit no response to an electric field. However, when reverse micelles are present, the particles move in a direction opposing the electric field, implying a negative charge. As the concentration of AOT increases from 0.8 to 200 mM, the magnitude of the mobility falls from 0.1 to 0.06 (μm/s)/(V/cm), as shown in Figure 5a.

We use these results to calculate the electrostatic potential at the surface of the particle. Since the screening length and particle radius are comparable, $\kappa a \approx 1$, we cannot ignore the polarization of the screening cloud and its drag effects. Therefore, to properly calculate the zeta potential from the electrophoretic mobility, we employ simultaneous, numerical solutions of the Poisson−Boltzmann and Navier−Stokes equations. We use the method of O'Brien and White, valid when applied electric fields are small compared to the fields inside the screening clouds.[25] The resulting values of the surface potential are plotted in Figure 5b. To emphasize that these values of the surface potential are obtained by electrokinetic measurements, they are labeled with the subscript EK. The error bars are large at high concentrations of AOT

(23) Parsegian, A. *Nature* **1969**, *221*, 844.
(24) Kotlarchyk, M.; Huang, J. S.; Chen, S. H. *J. Phys. Chem.* **1985**, *89*, 4382.
(25) O'Brien, R. W.; White, L. R. *J. Chem. Soc., Faraday Trans. 2* **1978**, *74*, 1607.

because the electrophoretic mobility is relatively insensitive to the surface potential at these ionic strengths. Our data are consistent with a surface potential that is independent of AOT concentration, $e\zeta_{EK}/k_BT = -5.5 \pm 0.2$ or equivalently $|\zeta_{EK}| = 140 \pm 5$ mV. This zeta potential is surprisingly large. In fact, it is comparable to measured values for highly charged aqueous colloids.[20] Inserting results from conductivity and electrophoresis measurements into eq 2, we find that the effective particle charge is about 200−900 electrons. While surface potentials in our system are comparable to highly charged aqueous systems, our particle charge is 1−2 orders of magnitude smaller.[20]

At first glance, the surface potentials implied by electrophoresis do not agree with those measured from interactions. In general, we observe $\zeta_{EK} > \zeta_{EQ}$. This apparent discrepancy is also found in aqueous colloids;[26] it arises because the analyses of our electrokinetic and interaction measurements do not employ mutually consistent definitions of the surface potential. Our analysis of electrophoresis measurements provides a value of the potential at the surfaces of the particles, consistent with the solution of the nonlinear Poisson−Boltzmann equation. Meanwhile, our interaction measurements probe the far-field regime where the electrostatic potential is low and the linearized Poisson−Boltzmann equation is accurate. The surface potential provided by fits to particle interactions, ζ_{EQ}, assumes that the linearized solution is valid all the way to the particle surface. However, since $|e\zeta| > k_BT$, this is not a valid assumption. In general, the apparent potential at far-field, ζ_{EQ}, is related to the potential at the surface of the sphere, ζ_{EK}, through the nonlinear Poisson−Boltzmann equation.

To relate our short- and long-ranged measures of the surface potential, we solve the nonlinear Poisson−Boltzmann equation to yield ζ_{EQ} as a function of ζ_{EK} and the ionic strength. We work in a spherical Wigner−Seitz cell whose radius is given by the volume fraction, $R = a\phi^{-1/3}$, subject to the boundary condition that the gradient of the electrostatic potential equals zero at the boundary. Using the methods of Alexander[26] and Trizac,[27] we extract the apparent far-field zeta potential and the effective ionic strength. Fixing the volume fraction and the surface potential, ζ_{EK}, we vary the ionic strength of the reservoir and calculate the apparent surface potential at far-field, ζ_{EQ}, versus effective κ. The results of this calculation for $\phi = 0.03$ and $|e\zeta_{EK}|/k_BT = 5.5$ are plotted against fitted values of ζ_{EQ} and κ_{EQ} in Figure 6b. The calculated trend is in quantitative agreement with values measured from suspension structure. Thus, the electrokinetic and structural measurements of particle surface potential and ionic strength are consistent.

By solving the nonlinear Poisson−Boltzmann equation, we have established the consistency of independent measurements of colloidal charge properties. Conductivity and electrophoresis measurements are well-established and essential to sample characterization in applications involving applied electric fields. Interaction measurements, while less established and more difficult to perform, determine colloidal stability and phase behavior. Interaction measurements offer a further advantage: by fitting $u(r)$ to the DLVO form, one can simultaneously extract the ionic strength and effective surface potential. These quantities can only be established from electrokinetic methods in well characterized systems, where the size and mobility of charge carriers has been independently established.

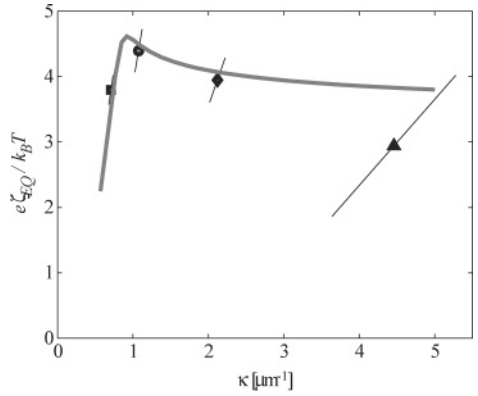

Figure 6. Comparison of electrostatic and electrokinetic measures of surface potential. The symbols represent fit parameters, $e\zeta_{EQ}/k_BT$ and κ_{EQ}, from interaction measurements. The error bars are off-axis because errors in ζ_{EQ} and κ_{EQ} are correlated. The solid line is a plot of the expected ζ_{EQ} based on the solution of the Poisson−Boltzmann equation and the measured value of the surface potential from electrophoretic mobility, $e\zeta_{EK}/k_BT = 5.5$.

E. Thermodynamic Model of Surface Potentials. We have shown that simple thermodynamic arguments can be applied to predict the ionic strength of our suspensions. We take a similar approach to understand surface potentials and find substanial deviations from aqueous systems. In order for a particle to charge, surface charges and their counterions must be created and separated. Thus, the energy required to charge a particle has three components. First, the counterion has a self-energy, g_M. Second, an ion on the particle's surface has a self-energy, g_S. Finally, once the ion and counterion have been created, they must be separated at an energy cost of $|e\zeta|$. To charge in equilibrium, these costs must be overcome by gains in entropy. In addition to the familiar configurational entropy of bulk ions, there is also the configurational entropy of charges on the particle surface. Although the entropic contribution of the surface is typically ignored in aqueous colloidal systems, we find that the unusual form of the bulk entropy in our systems amplifies its importance.

To determine the surface entropy, we consider the number of configurations of Z charges distributed over N chargeable sites on the surface of the particle. Since the charges are identical, the number of configurations is $\Omega = \binom{N}{Z}$. From Boltzmann's relation, $S = k_B \ln \Omega$. Applying Stirling's approximation, the change in free energy per unit charge due to surface charge configuration is thus $-T(dS/dZ) = k_BT \ln(Z/(N - Z))$. Therefore, when $Z \ll N$, the surface entropy's contribution to the chemical potential is $k_BT \ln[Z/N]$.

Ions in the bulk contribute a similar entropic term to the overall free energy of the system. The number of configurations is given by $\Omega = \binom{M-\chi M/2}{\chi M/2+Z}$, where M is the number of micelles per particle and $M - \chi M/2$ is the number of micelles available to accept counterions and like-charged excess ions. Applying Stirling's approximation again, we find that $-T(dS/dZ) = k_BT \ln((\chi M/2 + Z)/(M - \chi M - Z))$. In the limit where only a small fraction of micelles charge ($\chi \ll 1$) and excess ions dominate over counterions ($Z \ll \chi M$), bulk entropy's contribution to the chemical potential is $k_BT \ln(\chi/2)$. Alternatively, we can obtain this result by noting that when the particle charge increases by one, a neutral micelle in the bulk is converted to a charged micelle. If we model the neutral micelles and

(26) Alexander, S.; Chaikin, P. M.; Grant, P.; Morales, G. J.; Pincus, P.; Hone, D. *J. Chem. Phys.* **1984**, *80*, 5776.

(27) Trizac, E.; Bocquet, L.; Aubouy, M.; von Grunberg, H. H. *Langmuir* **2003**, *19*, 4027.

positively charged micelles as a mixture of ideal gases, the change in the free energy is $k_BT \ln[n_{ion}/2] - k_BT \ln[n_{micelle}] = k_BT \ln[\chi/2]$, where we have again assumed that only a tiny fraction of micelles are charged.

Combining the energetic and entropic contributions to the chemical potential,

$$\mu(Z) = g_S + g_M + e|\zeta| + k_BT \ln\left[\frac{Z}{N}\right] + k_BT \ln\left[\frac{\chi}{2}\right] \quad (4)$$

In equilibrium, $\mu = 0$. In the limit where excess ions dominate over counterions, $\chi = 2 \exp(-g_M)$, thus

$$e|\zeta| \approx -g_S - k_BT \ln[Z/N] \quad (5)$$

Remarkably, the bulk entropic contribution to the chemical potential exactly cancels the self-energy of the counterion. Consequently, the surface potential depends primarily on the competition between surface entropy and the self-energy of an ion on the surface. However, since Z depends on the ionic strength, eq 2, there is some residual dependence on g_M. Since the left-hand side is positive, definite, meaningful results are obtained only when $-\ln[Z/N] > g_S$. Therefore, surface entropy's contribution to the chemical potential must overcome the self-energy of a surface charge. This is in stark contrast to thermodynamic models of charging in aqueous systems, where the configurational entropy of the surface is typically ignored.[26]

In addition to highlighting the differences between aqueous and nonpolar systems, this thermodynamic picture allows us to estimate the self-energy of a charge on the particle surface, g_S, from our structural and electrokinetic measurements. Assuming that charges on the surface are constrained to reside within an adsorbed micelle, packing constraints limit the number of charges to 10^6. Our interaction measurements are consistent with $|e\zeta|/k_BT \approx 4$ and $Z \approx 100-1000$; therefore, $g_S \approx 3-5\ k_BT$, about one-quarter to one-half of the energy cost of charging an ion in bulk.

Combining our thermodynamic approaches to surface potentials and ionic strength, one may be able to predict the electrostatic interactions and electrokinetic response of nonpolar colloids from just a few material parameters: the ionization energy of ions in bulk and the number and ionization energy of chargeable sites on the particle surface. Thus, this thermodynamic model suggests a practical framework for rationally engineering the role of charge in nonpolar environments.

IV. Conclusions

Charge can play an important role in nonpolar colloids when reverse micelles are present to lower the electrostatic cost of ionization. The electrostatic interactions of these particles are surprisingly strong and tunable. Furthermore, the interactions between particles are consistent with values of the ionic strength and surface potential implied from electrokinetic measurements. While the functional form of interparticle potentials is identical to those of charged particles in aqueous solvents, the thermodynamics of charging is qualitatively different. Moreover, our results suggest new strategies for manipulating the stability, structure, and electrokinetic response of nonpolar colloids. We expect reverse micelle mediated colloidal interactions to become an invaluable tool in engineering nonpolar colloidal systems for industrial applications and fundamental research.

Acknowledgment. We thank Ian Morrison, Craig Herb, Phil Pincus, and Paul Chaikin for helpful discussions. We thank Infineum for the donation of equipment and E*Ink for access to their light scattering facilities. We also thank Sven Behrens and David Grier for the liquid structure theory code, Daniel Blair for help with the Monte Carlo simulations, and the Saville group for access to their electrokinetics code. We thank Andrew Schofield for providing the PMMA particles and PHSA stabilizer. We thank NASA (NAG 3-2284), the NSF (DMR-0243715), and the Harvard MRSEC (DMR-0213805) for funding.

LA046751M